

## FACTORS GOVERNING THE POST-PEAK HYSTERESIS LOOPS OF REINFORCED CONCRETE COLUMNS



Rajesh P. DHAKAL



Koichi MAEKAWA

The main aim of this study is to investigate the factors governing the post-peak cyclic response of laterally loaded reinforced concrete cantilever columns. A series of experiments are conducted, in which five reinforced concrete columns are subjected to cyclic lateral displacement. Much attention is paid to the cover concrete spalling and the large lateral displacement of the reinforcement. Specimens are designed so that the buckling of the reinforcement and the cover concrete spalling can be clearly observed. Finite element analyses are also performed using enhanced nonlinear fiber models. These analyses are verified by comparing their results with those of the experiments on the five RC columns.

**Keywords:** *axial compression, buckling, cover spalling, energy dissipation, post-peak softening*

---

Rajesh P. Dhakal is a research fellow in the Protective Technology Research Centre at the Nanyang Technological University, Singapore. He obtained his PhD from the University of Tokyo in 2000. His research interests cover constitutive modeling of reinforced concrete, seismic design of RC structures, and the structural response to explosion. He is a member of the JSCE and JCI.

---

Koichi Maekawa serves as professor in the Department of Civil Engineering at the University of Tokyo, Japan. He obtained his D.Eng. from the University of Tokyo in 1985. He specializes in nonlinear mechanics and constitutive laws of reinforced concrete, seismic analysis of structures, and concrete thermodynamics. He is a member of the JSCE and the JCI.

---

## **1. Introduction**

Reinforced concrete (RC) columns in civil engineering structures such as buildings and bridges are subjected to substantial axial compression from the combined weights of the overlying mass and the columns. Seismic design codes permit a wide range of longitudinal reinforcement ratios as well as cover concrete thicknesses for such columns. The seismic performance of such columns, especially in the post-peak range, also varies according to the number and arrangement of the longitudinal reinforcing bars and the axial load that is superimposed upon them. Hence, the post-peak behavior of RC columns is difficult to generalize, and a proper understanding of the interrelationships between the overall response and these parameters is needed.

This study focuses mainly on the cyclic response and energy dissipation capacity of RC columns in the post-peak range that accompanies spalling of the cover concrete and large lateral displacement of the longitudinal reinforcing bars (i.e., buckling). For this purpose, the authors intentionally selected details that induce large geometrical and material nonlinearity. Large covers and high axial compression are deliberately used to trigger spalling and buckling in order to investigate and clearly understand the influence of these inelastic material mechanisms on the post-peak cyclic response of RC columns. The above factors make less sense with actual large-scale RC columns because the thickness of the cover concrete and the size of the reinforcing bars are both relatively small and the axial force is not very high. These factors, however, are very influential on small-scale models in the laboratory, and prove the effect of size on the cyclic energy dissipation capacity that is associated with the buckling of longitudinal reinforcing bars and spalling of cover concrete. It is important to recognize this aspect, especially when trying to understand the response of actual RC columns based on the small-scale laboratory models. The authors have tried to address this point with special consideration of the details of the experiments, which are not usually seen in actual structures but are meaningful for investigating the specific problems concerned.

Energy dissipation capacity, defined as the capacity of structures to dissipate externally applied energy, is an important parameter for judging the seismic performance of RC structures. The usual intention of the designer is to create a structure with higher energy dissipation capacity as this reduces the possibility of a brittle and explosive failure that might be fatal during earthquakes. Nevertheless, it is not easy to precisely determine in advance the post-peak response and the energy dissipation capacity of the designed structure as these are influenced by many factors, including spalling of the cover concrete, and geometrically large local deformation of the reinforcement.

However, the energy dissipation capacity can be determined from the area enclosed by the load-displacement curve during one cycle of unloading and reloading. Obviously, it is greatly influenced by the pinching mechanism, which can be observed in the cyclic load-displacement curve of RC structures. The main sources of this pinching mechanism are thought to be reinforcement pullout and bond-slip at the column-footing joint accompanying the shear slip along the joint planes between the column and the footing. Moreover, shear deformation of the column also contributes to pinching behavior, as the lateral load versus shear deformation relationship shows severe pinching with negligible residual deformation during unloading and/or reloading. It is believed that preventing shear deformation, reinforcement pullout, bond-slip, and joint plane slip will result in a cyclic response with very little pinching and consisting of large hysteresis loops, indicating a high energy dissipation capacity.

In contrast to expectations, the response of flexural columns with less bond-slip and negligible pullout also proved capable of exhibiting pinching, which reduces the energy dissipation capacity during cyclic response [1]. This study explores the factors causing such behavior during cyclic response of RC columns and investigates through experiments and analyses the qualitative interrelationship between these factors and the overall response. Here, thick covers and high axial compression are the key points.

## 2. Lateral cyclic loading tests of RC columns

### 2.1 Test setup and specimen details

An experiment was conducted on five RC columns to study the cyclic behaviors of laterally loaded reinforced concrete cantilever columns. The specimens had the same dimensions but they differed in the amount and arrangement of the longitudinal and lateral reinforcing bars, the thickness of the cover concrete and the amount of axial compressive stress. The test setup and the layout of the specimens are shown in Figure 1, and the geometrical and mechanical properties of all five specimens are tabulated in Table 1. Columns 1 and 2 represent columns with normal cover thicknesses and reinforcement ratios, but the axial stress in column 1 is 4 MPa whereas no axial compression is applied to column 2. Similarly, columns 3 and 4 represent columns with normal reinforcement ratios but the reinforcing bars are placed only at the center so that the thickness of

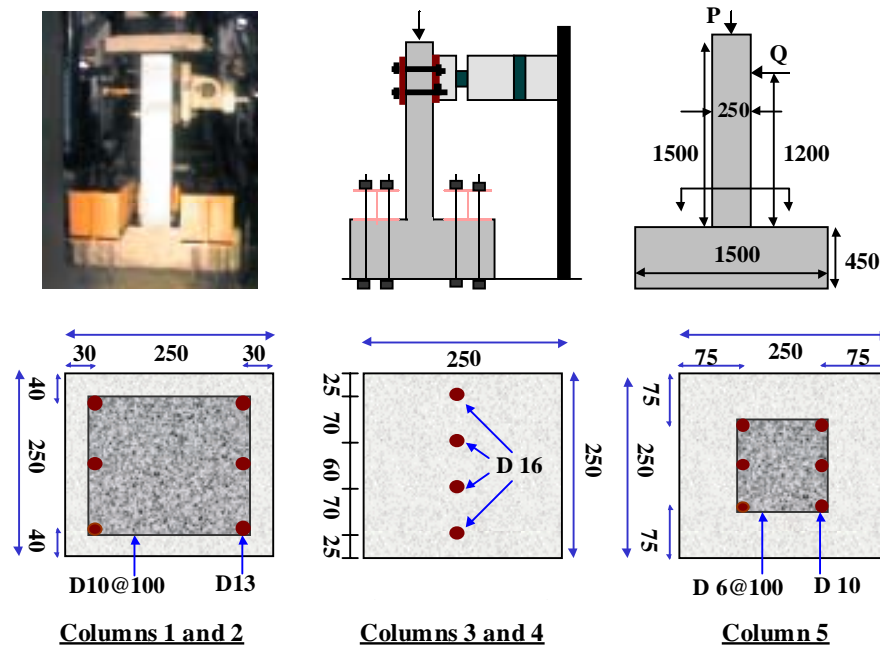


Figure 1 Test set-up and specimen details (Unit: mm)

Table 1 Geometrical and mechanical properties of specimens

|                                  | Column 1 | Column 2 | Column 3 | Column 4 | Column 5 |
|----------------------------------|----------|----------|----------|----------|----------|
| Cross section, mm                | 250×250  | 250×250  | 250×250  | 250×250  | 250×250  |
| Main reinforcement               | 6-D13    | 6-D13    | 4-D16    | 4-D16    | 6-D10    |
| Lateral ties, mm                 | D10@100  | D10@100  | -        | -        | D6@100   |
| Reinforcement ratio              | 1.216%   | 1.216%   | 1.271%   | 1.271%   | 0.685%   |
| Concrete cover, mm               | 30       | 30       | 125      | 125      | 75       |
| Axial stress, MPa                | 4.0      | 0        | 4.0      | 0        | 4.0      |
| Shear span, mm                   | 1200     | 1200     | 1200     | 1200     | 1200     |
| $f_c'$ , MPa                     | 28.6     | 28.6     | 29.7     | 29.7     | 38.2     |
| $f_y$ , MPa                      | 365      | 365      | 365      | 365      | 370      |
| $E_s$ , GPa                      | 202      | 202      | 200      | 200      | 195      |
| Shear capacity, V (kN)           | 131.9    | 127.4    | 44.68    | 29.55    | 80.80    |
| Flexural capacity, $V_{mu}$ (kN) | 43.61    | 24.15    | 33.91    | 24.68    | 33.18    |
| Capacity ratio, $V/V_{mu}$       | 3.02     | 5.27     | 1.32     | 1.20     | 2.44     |

the cover concrete is half the width of the corresponding columns. Moreover, the values of axial compressive stresses in these two columns are also different (4 MPa and 0 MPa, respectively). In addition, column 5 has a relatively smaller reinforcement ratio and larger cover thickness whereas the axial compressive stress is 4 MPa. It should be noted that RC columns with reinforcing bars only at the center are highly unusual. The specimens used in this experiment were specially designed to allow close observation of the local and geometrical nonlinearities associated with reinforcement and concrete, which significantly influence the cyclic response of reinforced concrete in the post-peak inelastic region.

In order to avoid shear failure, all five columns were designed so that the shear capacity would be sufficiently higher than the flexural capacity. The columns were cast monolithically with rigid footings and were subjected to cyclic lateral displacement under constant axial compression. Axial compression was applied at the top of the columns and cyclic lateral displacement was applied at a height of 120 cm from the top face of the footing. Each displacement cycle was repeated twice to observe the load degradation. A triaxial loading machine was used so that axial compression and lateral displacement could be applied simultaneously. In order to make the columns function as cantilever beams, the footings were tightly fixed to the base slab using prestressed tendons. The strains of the reinforcing bars and extreme concrete fibers near the footing were measured using strain gauges. Similarly, the displacements at the loading point and the opening at the column-footing joint due to pullout of reinforcing bars from the footing were also recorded with the help of displacement transducers.

## 2.2 Post-peak cyclic response

### 2.2.1 Columns 1 and 2

The experimental load-displacement curve and the observed crack pattern of column 1 are shown in Figure 2. In the experiment, uniform flexural cracks appeared gradually and the behavior was governed by the crack nearest to the footing. During cyclic loading, this crack alternately opened and closed and after a few cycles the cover concrete spalled near the column-footing joint. The spalling at the base of the column occurred when the applied displacement reached approximately 15 mm. After the experiment, the spalled cover concrete was removed, revealing slightly buckled reinforcing bars.

However, the starting point of the buckling could not be determined. Once the cover concrete had spalled, the post-peak load-displacement curve showed a gradual decrease in the lateral load, and the ductility ratio was not very large. It can be argued that the decrease in the lateral load in the post-peak region was caused by the P-delta effect. But the softening observed in Figure 2 (column

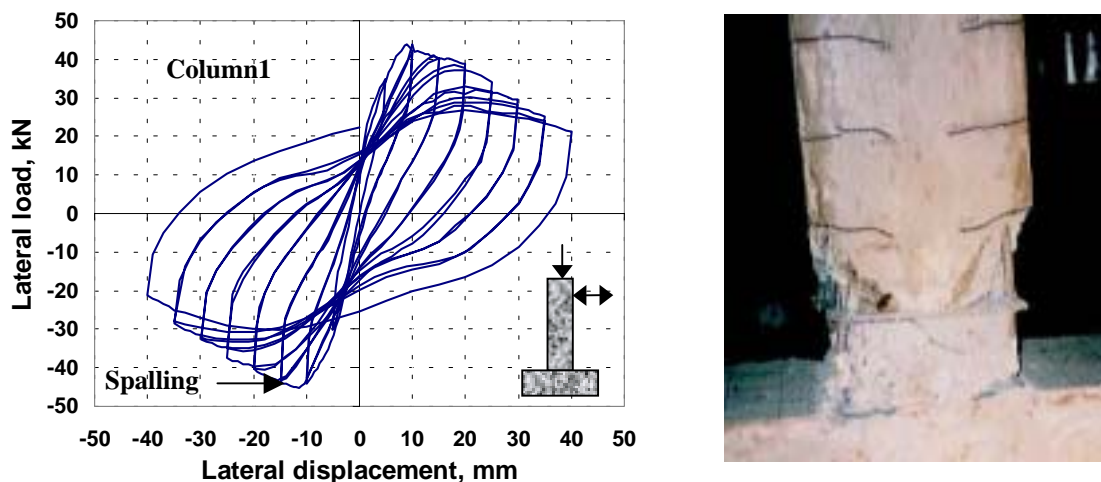
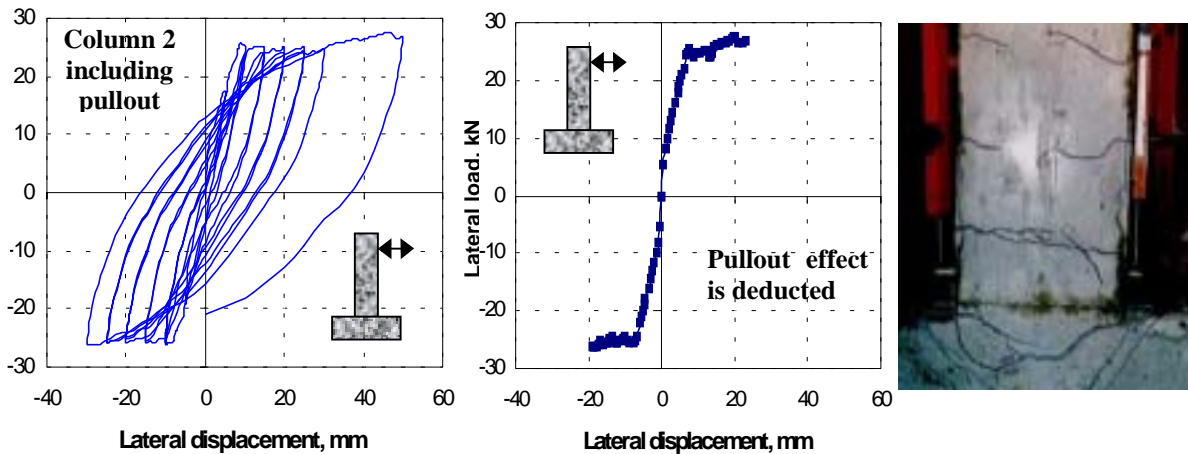


Figure 2 Load-displacement curve and crack pattern of column 1



**Figure 3** Load-displacement curve and crack pattern of column 2

1) is not due solely to the P-delta effect. For example, the decrease in the lateral load from 10 mm to 40 mm was around 20 kN, but the contribution of the P-delta effect was only 6.25 kN ( $250 \text{ kN} \times 30 \text{ mm} / 1200 \text{ mm}$ ). It was also found that because of the axial compression (14% of the axial capacity), there was little reinforcement pullout at the base. The two cycles for the same displacement produced nearly identical responses, and a small amount of load degradation could be observed only in the high-displacement cycles. The experimental response shows a significantly large energy dissipation capacity with slight pinching during unloading and reloading.

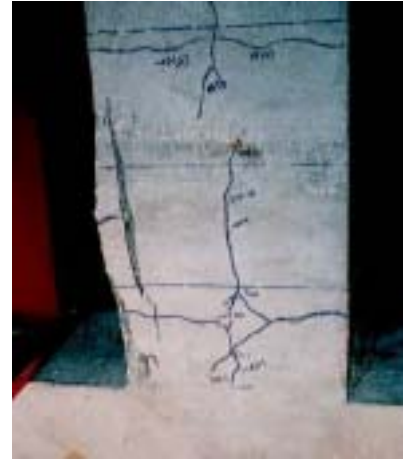
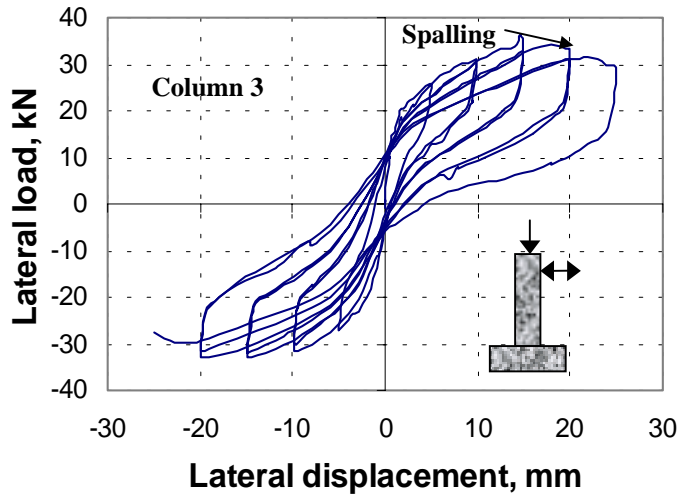
Figure 3 shows the experimental load-displacement curve and observed crack pattern on a similar column tested without axial compression (column 2). Inclined cracks started forming at the column-footing joint. Under cyclic loading, the inclined cracks from two sides merged as shown in Figure 3. During further loading, these cracks opened and closed to a large extent. Although other flexural cracks appeared above the column-footing joint, the behavior was mainly governed by these inclined cracks. Note that columns 1 and 2 were geometrically identical yet no inclined cracks at the column-footing joint were observed in column 1. The only difference was the absence of axial compression in column 2. However due to no axial compression, there was pullout of the reinforcing bars at the column-footing joint, which caused prominent inclined cracks at the base in addition to the regularly spaced flexural cracks.

Figure 3 also shows the load-displacement curve after deducting the top displacement due to the reinforcement pullout at the column-footing joint. It can be observed that pullout contributed approximately 30-40% of the top displacement in the high-deformation range. As expected, cover concrete spalling and reinforcement buckling did not occur, and there was no softening in the load-displacement relationship even in the high-displacement range. Consequently, there was pronounced ductility, and cyclic response showed a higher energy dissipation capacity with no pinching. The two cycles for the same displacement produced the same response, and no load degradation could be observed even in high-displacement cycles.

In both specimens, cracks in the two directions were nearly symmetrical and the location and spacing of the cracks in both cases were identical to those of lateral ties. Because the specimens were designed to have comparatively higher shear strength, no diagonal shear cracks were seen.

#### 2.2.2 Columns 3 and 4

The experimental load-displacement curve and observed crack pattern for column 3 are shown in Figure 4. Flexural cracks initiated from the face of the column slightly above the footing. Under cyclic loading, these cracks from two sides opened and closed alternately. During further loading, a vertical splitting crack developed in the side surfaces along the position of the longitudinal reinforcing bars. This vertical splitting crack bridged the two bending cracks as shown in Figure 4.



**Figure 4** Load-displacement curve and crack pattern of column 3

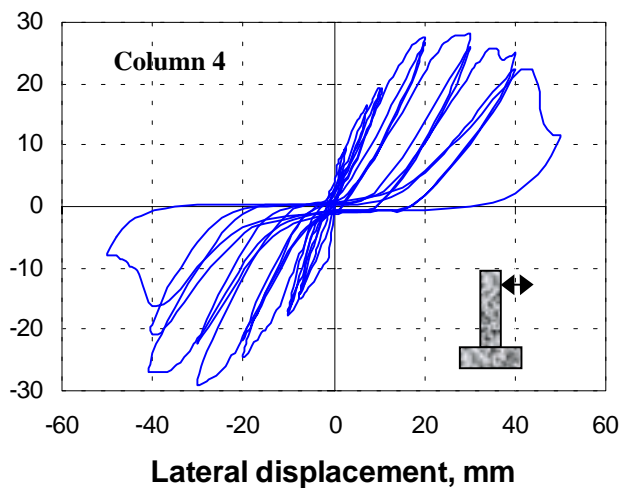


**Figure 5** Load-displacement curve and crack pattern of column 4

Cover concrete spalling could be partially observed when the applied displacement exceeded 20 mm. As the reinforcing bars were placed only at the center, complete cover spalling and buckling of reinforcement did not take place and due to the large axial compressive stress, pullout of the reinforcing bars was not observed. After the partial spalling of the cover concrete, the lateral load in the post-peak load-displacement curve decreased slightly. After the applied displacement reached 25 mm, the column became unstable and the loading was terminated. The experimental response shows comparatively less energy dissipation capacity because of the high pinching behavior, and the load at zero displacement during unloading and reloading was about 20% of the maximum load.

Figure 5 shows the experimental load-displacement curve and observed crack pattern for a similar column that was not subjected to axial compression (column 4). Flexural cracks initiated from the column-footing joint. Under cyclic loading, the cracks from the two sides merged and alternately opened and closed. Later, another pair of bending cracks emerged from a height of about 30 cm from the top of the footing. A vertical splitting crack developed along the position of the longitudinal reinforcing bars and bridged the two bending cracks as shown in Figure 5. As the reinforcing bars were placed only at the center and no axial compression was applied, cover spalling and reinforcement buckling did not occur. After high displacement, which exceeded 40 mm, was applied, the concrete on the compression side crushed and the column lost its capacity to

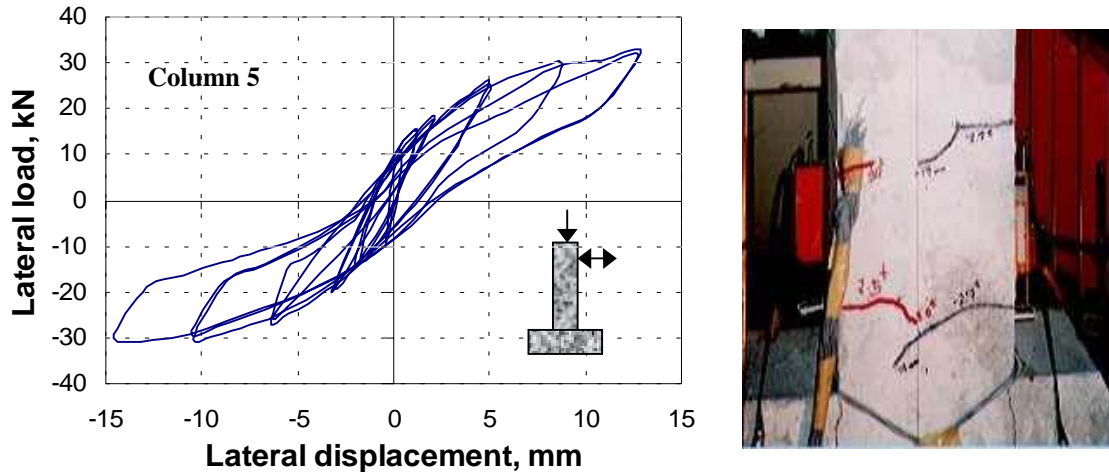


**Figure 6** Load-displacement curve and crack pattern of column 5

carry further load, as suggested by the sudden drop in the load in the later stage of the load-displacement relationship. The load-displacement curve passed through the origin and the load at zero displacement during unloading and reloading was found to be very close to zero.

In both cases, the bending cracks were localized and the spacing between the two bending cracks in both specimens was greater than the section size. This was due to the absence of reinforcement in the vicinity of the column faces, from where these discrete cracks were generated. Near the reinforcing bars around the center, however, smeared cracks could be seen in the side surfaces. Moreover, the crack pattern was nearly symmetrical, and because the specimens were designed to have comparatively higher shear strength, no diagonal shear cracks could be seen.

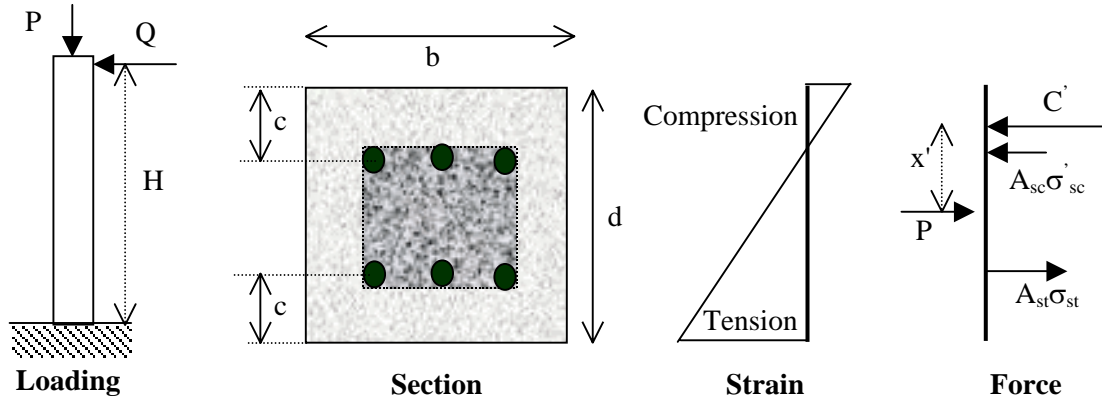
### 2.2.3 Column 5

Figure 6 shows the experimental load-displacement relationship and observed crack pattern for column 5 (with a thick cover, smaller reinforcement ratio and significant axial stress). As the applied displacement was small, only two pairs of bending cracks were observed. The applied displacement could cause yielding of the reinforcement but it was not sufficient to cause cover spalling and reinforcement buckling. The figure shows that, unlike the response of normal structures, the load-displacement curve has smaller residual displacement during unloading and reloading and the energy dissipation capacity is smaller due to substantial pinching.

### 3. Factors influencing the post-peak cyclic response

The extent of the pinching and the energy dissipation capacity can be explained in terms of the load at zero displacement during unloading or reloading from the peak displacements in both extremes. For example, a small energy dissipation capacity implies that the load at zero displacement is smaller than is in the case of a higher energy dissipation capacity. The load at zero displacement depends on the cyclic behavior of the constituent materials; i.e., concrete and reinforcing bars. It is well known that the cyclic response of reinforcing bars shows wider cyclic loops with higher energy dissipation capacities due to yielding. In contrast, the cyclic loops of concrete response exhibit high pinching, and the load at zero displacement during unloading and reloading is close to zero. Consequently, the energy dissipation capacity of RC structures depends on the relative contributions of the longitudinal reinforcing bars and the concrete to the overall response.

Figure 7 shows the general features of a laterally loaded reinforced concrete column under axial compression. A cantilever reinforced concrete column with a rectangular cross-section (width  $b$  and depth  $d$ ) under constant axial compression  $P$  is subjected to lateral displacement  $\delta$  at a height  $H$



**Figure 7** Section analysis for RC response

above the fixed support. By calculating the moment  $M$  induced by externally applied loads at the base of the column, equation (1) can be obtained, where  $Q$  is the lateral load corresponding to the applied displacement. Geometrical nonlinearity can be incorporated by considering the P-delta moment in equation (1).

$$Q = \frac{(M - P\delta)}{H} \quad (1)$$

Figure 7 also includes the strain distribution across the cross-section as well as the sectional forces carried by concrete and reinforcing bars. Here, the contribution of the concrete to the tension is neglected and linear strain distribution is considered across the cross-section. This assumes that the plane section remains plane after bending. As shown in equation (2), the sectional moment at the base of the column can be calculated by accumulating the moments about the centerline due to all of the sectional forces. Similarly, equation (3) is derived from the equilibrium between the axial load and the sectional forces carried by the concrete and reinforcing bars.

$$M = A_{st}\sigma_{st}\left(\frac{d}{2} - c\right) + A_{sc}\sigma'_{sc}\left(\frac{d}{2} - c\right) + C'x' \quad (2)$$

$$C' = P + A_{st}\sigma_{st} - A_{sc}\sigma'_{sc} \quad (3)$$

In equations (2) and (3), the areas of reinforcing bars in tension and compression sides are denoted respectively by  $A_{st}$  and  $A_{sc}$ , and the stresses in the corresponding reinforcement are symbolized by  $\sigma_{st}$  and  $\sigma'_{sc}$ , respectively. The distance to the center of the reinforcing bars from the edge (slightly larger than the clear cover thickness) is denoted by  $c$ , and  $C'$  is the resultant of the sectional compressive forces carried by the concrete. Similarly,  $x'$  represents the distance from this resultant to the center of the section, where the axial load is supposed to act. The first two terms on the right hand side of equation (2) represent the contribution of the reinforcement to the overall response, whereas the last term, along with equation (3), represents the contribution of the concrete. As suggested by equation (2), the relative contribution of the reinforcement to the overall response depends upon the location and number of longitudinal reinforcing bars. Similarly, equation (3) shows that the contribution of the concrete to the overall response depends upon the axial load as well as the reinforcement ratio.

Equation (2) also explains the effect of the material models in the post-peak response envelope for RC columns. The stresses carried by the reinforcing bars and concrete increase up to the point of peak loading because the reinforcing bars are in the elastic or hardening phase and the concrete has not reached the compression-softening phase. But in the post-peak region, the compressive strains in the reinforcing bars and concrete are sufficiently high to cause spalling of the cover concrete and

a large lateral displacement (i.e., buckling) of the reinforcement. The average compressive stress carried by the reinforcement in the post-buckling phase significantly decreases, and the cover concrete completely loses its load-carrying capacity after spalling [2]. Because of these inelastic material mechanisms, the post-peak response of RC columns might show softening, depending upon the level of the compressive strains in the concrete and the reinforcing bars. These strains are greatly influenced by the level of axial compression and the thickness of the cover concrete. This means that material models must take into account spalling and buckling before the models can reliably predict post-peak response.

According to equation (2), the thicker the cover concrete, the smaller the contribution of the reinforcement would be. The position of the reinforcing bars also influences the reversal of the stress in the reinforcing bars and concrete, which significantly influences the cyclic response of RC columns. The closer the reinforcing bars to the centerline, the smaller the induced maximum compressive stress would be, resulting in incomplete reversal of the stress. This produces comparatively smaller values for the reinforcement stresses  $\sigma'_{sc}$  and  $\sigma'_{st}$ , both of which tend to be tensile in nature, further reducing the moment carried by the reinforcing bars. As suggested by equation (3), this tendency again increases the sectional force carried by the concrete, thus rendering the overall cyclic response closer to the cyclic behavior of concrete. In extreme cases, when the cover thickness is equal to half the column depth, equation (2) shows that the contribution of the reinforcement is zero and the overall response is completely governed by the concrete, regardless of the reinforcement ratio and corresponding stresses. Similarly, if the reinforcement ratio is reduced, the sectional forces carried by the reinforcing bars are reduced and their contribution to sectional moment also becomes smaller. As a result, the concrete contribution to the overall response increases and the cyclic behavior shows greater pinching and a smaller energy dissipation capacity.

If there is no axial compression, the resultant  $C'$  of compressive forces, carried by the concrete fibers at zero displacement during unloading and reloading, is nearly zero and is located very close to the centerline. In other words,  $x'$  is small. Since equation (3) should always be satisfied, the stresses in the reinforcing bars on the tensile and compressive side ( $\sigma'_{st}$  and  $\sigma'_{sc}$ ) are opposite in nature because the axial load  $P$  is zero and the resultant of concrete compression  $C'$  at zero displacement is also small. This tendency increases the contribution of reinforcement to the section moment, and the overall cyclic response of such columns becomes very close to the cyclic behavior of the reinforcing bars, showing larger loops with a higher energy dissipation capacity. On the other hand, if a high axial load is applied, there is significant compressive strain with a very small strain gradient throughout the cross-section even at zero displacement. The high axial load induces compressive stresses in the reinforcing bars on both sides, which reduces the contribution of reinforcement to the section moment. As a result, the sectional force carried by the concrete becomes greater, and concrete contribution to the overall response increases. Hence, the overall cyclic response of such columns is closer to the cyclic behavior of concrete, showing greater pinching and a smaller energy dissipation capacity.

#### **4. Nonlinear analysis of RC columns**

##### **4.1 Material models for FEM analysis**

A three-dimensional and nonlinear finite-element analysis program called COM3 (*Concrete Model in 3D*) is used to analytically predict cyclic behavior of RC columns. In COM3, the columns are represented by frame elements, which are analyzed using fiber technique [3][4]. In fiber technique, each element is represented by a single line coinciding with the centerline of the member. The member cross-section is divided into many cells or sub-elements. The strain of each cell is calculated using Euler-Kirchoff's hypothesis, which states that a plane section remains plane after bending. The stress carried by each fiber is calculated from the axial strain in that fiber using the material models that represent the average stress-strain relationship. As is well known, the overall

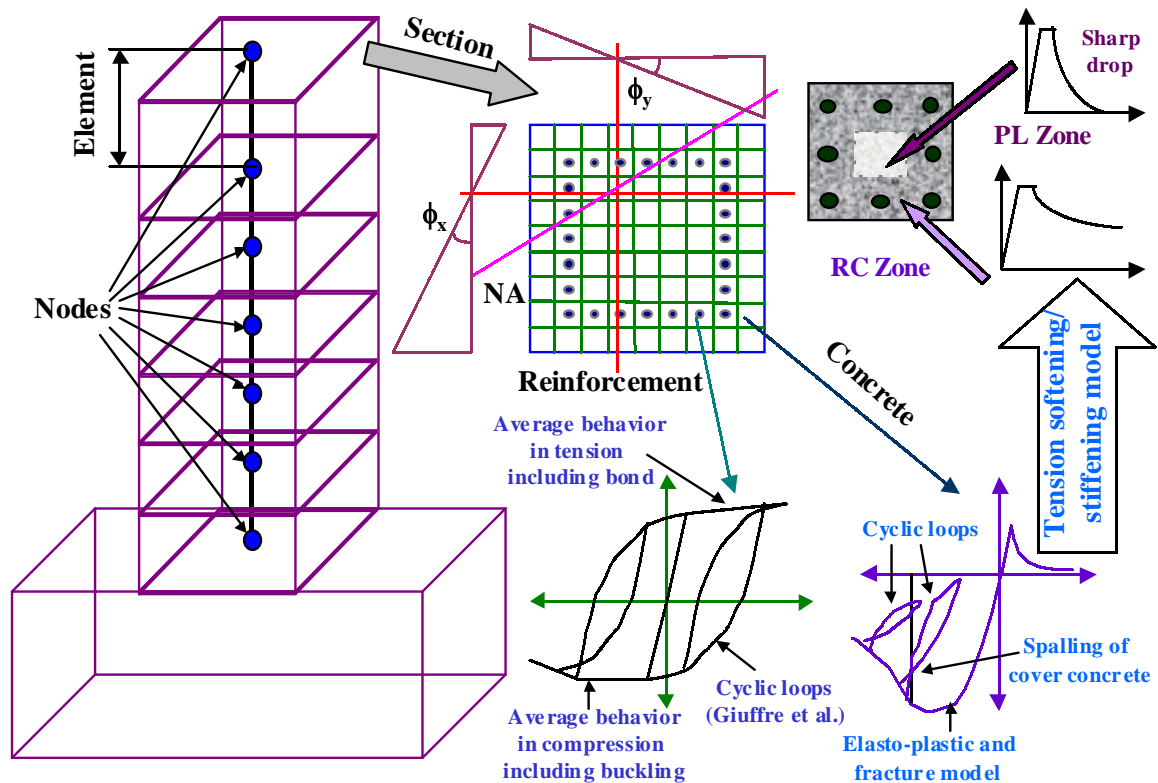


**Figure 8** Fiber technique and material models

response of each element is the integrated response of these fibers and the overall response of the member comprises all of the element responses.

In fiber technique, the stress field is reduced to one dimension along the axis of a finite element or member. The shear force is then computed so that it is in equilibrium with the flexural moment field. The out-of-plane shear failure is not inherently captured due to degenerated formulation of the stress field adopted for the sake of simplicity. In-plane shear deformation is considered, however, using Timoshenko's beam theory. Conclusively, if the shear strength of the concerned structure is high enough to ensure flexure failure, the performance of the fiber technique is sufficiently reliable to analytically predict flexural behavior.

Figure 8 shows the schematic representations of fiber technique as well as the material models used for concrete and reinforcement in each fiber. The models for concrete consist of the *elasto-plastic and fracture model* [5] combined with the cover concrete spalling criteria for concrete in compression and the *tension softening model* for concrete in tension, which includes the effects of RC and PL zones [6]. Similarly, the models for reinforcing bars incorporate the average stress-strain relationship, including the effect of buckling during compression and the effect of bond during tension [7]. For the cyclic behavior of reinforcing bars, the equations proposed by Giuffre-Menegotto-Pinto [8] are used to represent the Bauschinger effect. For concrete, path-dependent cyclic curves [7] are used in the analysis. All of these models are path-dependent and include loading, unloading and reloading conditions. They have been satisfactorily verified at the element and member levels, and have been incorporated into COM3 to permit analysis of reinforced concrete under monotonic, cyclic and seismic loading.

#### 4.2 Mesh size independent average models

In FEM analysis of RC structures, the members are discretized into several elements that are analyzed using constitutive models representing an average stress-average strain relationship.

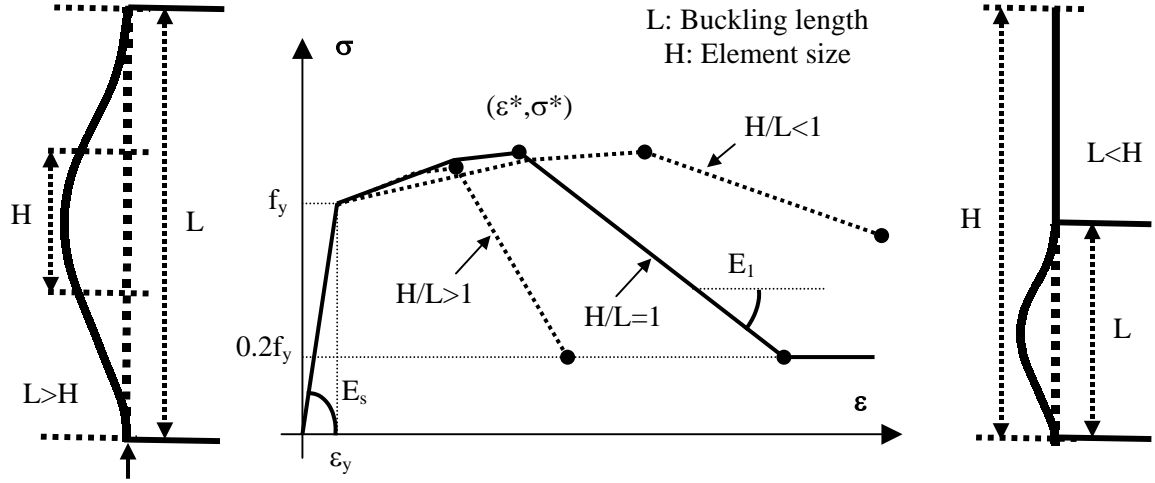


**Figure 9** Effect of element size in average compression behavior

These smeared material models calculate the average stress in each element corresponding to the spatially averaged strain throughout the element domain. The tri-linear relationships (Figure 9) between the average compressive stress and the average compressive strain within the buckling length of a reinforcing bar are described by equation (4).

$$\frac{\sigma}{\sigma_l} = 1 - \left(1 - \frac{\sigma^*}{\sigma_l^*}\right) \times \left(\frac{\varepsilon - \varepsilon_y}{\varepsilon^* - \varepsilon_y}\right); \quad \text{for } \varepsilon_y < \varepsilon \leq \varepsilon^* \quad (4)$$

$$\sigma = \sigma^* - 0.02E_s(\varepsilon - \varepsilon^*); \quad \text{for } \varepsilon > \varepsilon^*$$

$$\sigma \geq 0.2f_y;$$

In equation (4),  $\sigma_l$  and  $\sigma_l^*$  are the local stresses corresponding to  $\varepsilon$  (current strain) and  $\varepsilon^*$  (strain at the intermediate point), respectively. Similarly,  $\varepsilon_y$  and  $E_s$  are the yielding strain and Young's modulus of the reinforcing bar. The coordinates of the intermediate point  $(\varepsilon^*, \sigma^*)$  can be calculated as shown in equations (5) and (6). In these equations,  $L/D$  is the slenderness ratio,  $f_y$  is the yield strength of the reinforcing bar in MPa, and  $\alpha$  is a constant.

$$\frac{\varepsilon^*}{\varepsilon_y} = 55 - 2.3\sqrt{\frac{f_y}{100} \frac{L}{D}}; \quad \frac{\varepsilon^*}{\varepsilon_y} \geq 7 \quad (5)$$

$$\frac{\sigma^*}{\sigma_l^*} = \alpha \left(1.1 - 0.016\sqrt{\frac{f_y}{100} \frac{L}{D}}\right); \quad \sigma^* \geq 0.2f_y \quad (6)$$

$$\varepsilon_p^{sp} = \frac{a_{cr}^2 \pi^2}{4L^2} \quad (7)$$

Equation (7) calculates the plastic compressive strain in longitudinal reinforcing bars that causes spalling of the surrounding cover concrete. Here,  $L$  is the buckling length determined by stability analysis [9] and  $a_{cr} = (4+k) G_f / f_t$  is the splitting crack width, where  $k$ ,  $G_f$  and  $f_t$  are the fracture parameter in the *elasto-plastic and fracture model* [5], the fracture energy, and tensile strength of the concrete, respectively. Note that the average strains in the buckling and spalling models

represent the spatially averaged values of local strains within the buckling length of longitudinal reinforcing bars. Hence, if the element size is equal to the buckling length, these models can be directly applied with perfect consistency. Nevertheless, the size of the element in the FEM mesh of RC members is not necessarily always equal to the buckling length. One can expect larger or smaller elements depending on the overall size of the structure and the nature of the problem. In such cases, the spalling and buckling models need slight modifications if they are to be consistently applied to finite element analysis.

Figure 9 is a schematic representation of the influence of relative element size on the average compressive strain. Two cases are cited in the figure: one case with a buckling length greater than the element size, and one case with a buckling length smaller than the element size. The local strain profile is highly irregular within the buckling length, while the other parts of the reinforcing bar, which do not undergo lateral deformation, have equal and uniform strain. When the element size is greater than the buckling length, the average strain of the straight part is smaller than the average strain of the buckled part. Hence, the average strain in an element will be smaller than the average strain within the buckling length. In other words, even a smaller average strain in large elements is sufficient to cause large local strain resulting in earlier spalling and buckling. In contrast, the average stress becomes closer to the local stress as the element size becomes smaller compared with the buckling length. Consequently, the average element strain is larger than the average strain within the buckling length. It means that a larger average strain is required in small elements to cause local buckling of the reinforcement and spalling of the cover concrete. The effect of the relative size of the element and the buckling length in an average compression stress-strain relationship is also shown in Figure 9.

It is understood that the average strain is the same as the local strain in the elastic range, irrespective of the element size. The average strain in the post-buckling region, however, is sensitive to the mesh size. To qualitatively incorporate this mesh size sensitivity, the element-based average plastic strain of the reinforcement is obtained as the product of the average plastic strain within the buckling length and the square of the ratio of the buckling length to the element size. Thus the calculated average strain in the element domain is used in the buckling and spalling models. Moreover, the softening stiffness in the buckling model is also multiplied by the square of the ratio of the element size to the buckling length. This mesh size consistency in terms of the buckling of reinforcing bar is performed on the same line of tension based fracture model [7]. The second power (of the  $L/H$  ratio) is not exact but has been found to provide better consistency as shown by the verification in the next chapter. If the deformation is completely confined to within the buckling length or element length, whichever is smaller, and no deformation occurs in the other parts, then  $L/H$  gives an exact transformation. As strain exists throughout the reinforcement axis, this multiplication factor is not necessarily equal to  $L/H$ . Due to the nonlinear nature of the strain distribution, the exact determination of this coefficient is rather complex and presents a challenging problem to be addressed in the future.

To check the performance of the aforementioned method of eliminating size sensitivity in finite element computation, fiber analysis is performed with and without considering size sensitivity. The geometrical details of the laterally loaded cantilever column used for this purpose are shown in Figure 10. The yield strength and Young modulus of D19 steel bars are assumed to be 300 MPa and 200 GPa, respectively. The compressive strength of the concrete is assumed to be just 2 MPa. The small strength value is intentionally assumed so that the reinforcement model in compression governs the flexural behavior of the column, and the proposed mesh size independent compression model of reinforcement can be directly verified. The concrete material model is

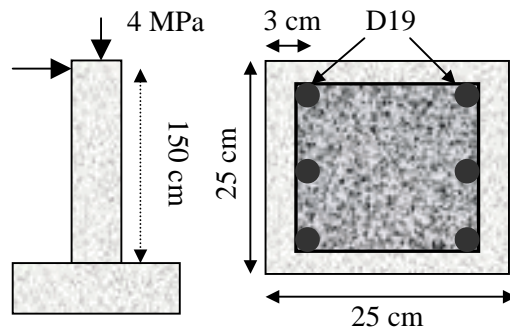


**Figure 10** Specimen for verification of mesh-size sensitivity

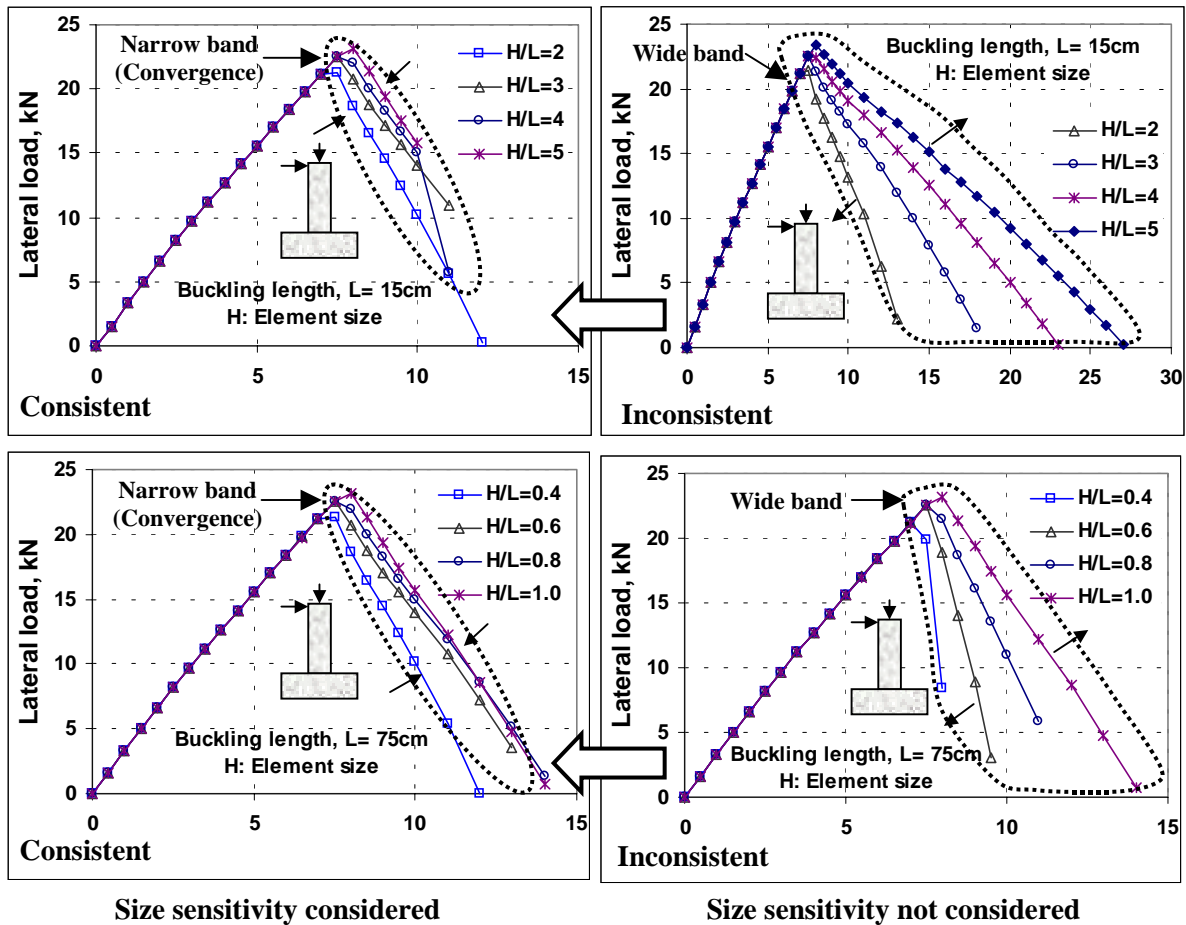


**Figure 11** Verification of mesh-size consistent computation

also affected by the element size. However, due to the small value for the strength of the concrete, the result is unaffected by the size effect of the concrete. This fictitious column was chosen just for computational verification and does not represent the standard RC columns used in real structures. In order to study element size sensitivity in normal RC columns, the size effect in the concrete model should also be properly addressed.

A constant axial compressive stress equal to 4 MPa was applied to this fictitious RC column, which was again subjected to monotonic lateral displacement at the top. The column was discretized into small finite elements that were analyzed using fiber technique. The size of the bottommost element, which governs the overall flexural behavior, was varied in order to investigate size dependency. Two sets of analyses were conducted, one for a buckling length of 15 cm and one for a buckling length of 75 cm, so that the element size would be respectively larger and smaller than the buckling length. The results of these analyses are shown in Figure 11.

As expected, compression yielding and buckling occurred before cracking and tension yielding, and the overall behavior closely followed the compression model for the reinforcement used in the analysis. It can be observed that in the case where the ratio of element size to buckling length was small, the post-peak load showed rapid degradation when the average stress-strain relationship based on buckling length was directly applied. This is because the smaller the element size, the larger the effect of strain localization on the average strain in the element domain would be. Once the average compression model is adjusted to rationally represent the average behavior within the element domain, the computed post-peak responses are nearly unique. It verifies that the proposed modifications successfully make the average compression model independent of the finite element size.

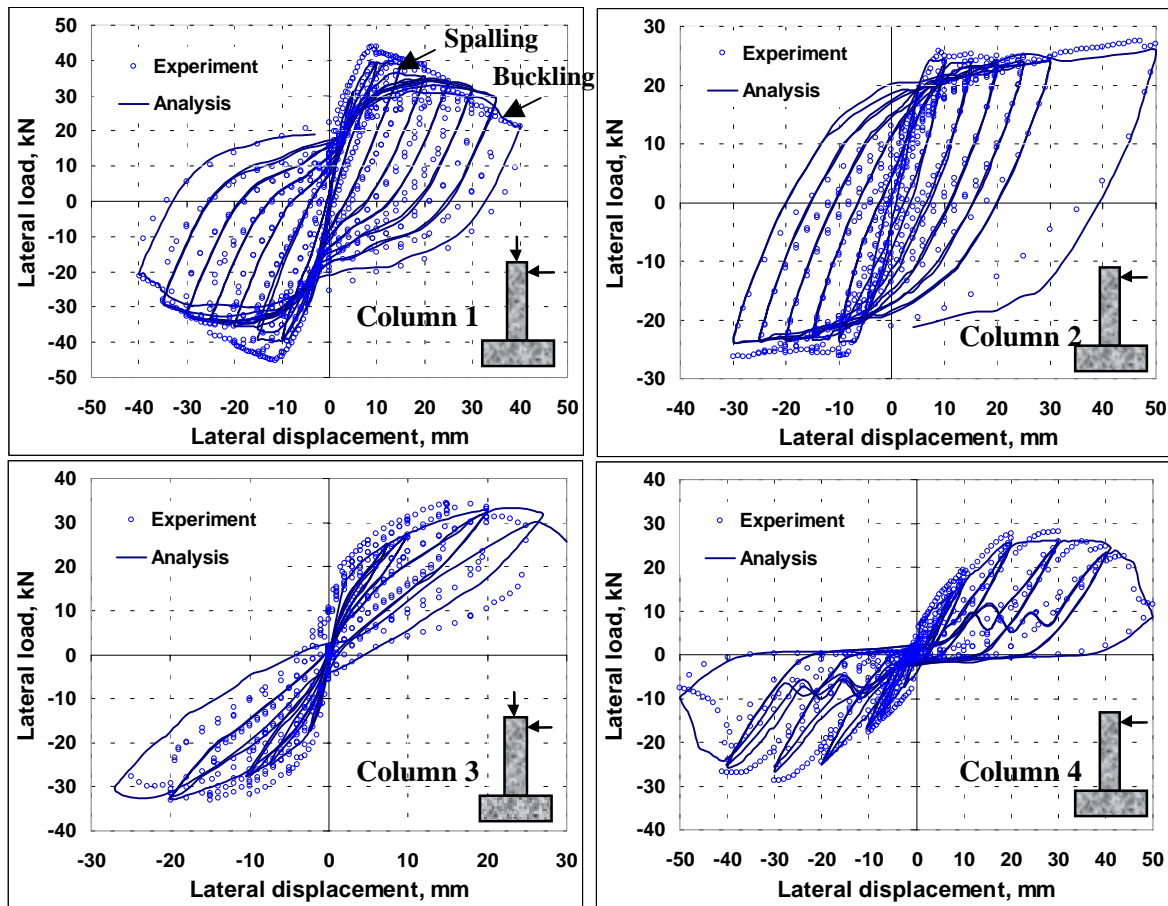


**Figure 12** Member level verification of analytical results of tested columns

However, a small difference in the yielding load can be seen in the computed responses for different element sizes. This difference is rooted in the basic principle of finite element formulation; i.e., the element response is calculated based on some referential gauss points, the positions of which vary proportionally to the element size. Consequently, the bottommost gauss point shifts upward if a larger element is used at the bottom and the yielding load is slightly overestimated. Although size dependency at the element level can be avoided by using models independent of mesh size, some effect of element size still remains at the structural level. It is therefore recommended that very large element sizes not be used in the sensitive region, where the maximum moment occurs.

#### 4.3 Analytical results and verification

Using fiber technique and the aforementioned material models, the five RC columns were analyzed and the analytical results compared with the experimental results for verification at the member level. Each column was represented by five frame elements, each 30 cm long, and the cross section was divided into more than 200 cells. In other words, one element consisted of more than 200 fibers. As the footing and the connections were sufficiently rigid during the experiment, the footing was not explicitly considered in the analysis, and a fixed support was provided at the base of the column. In case of axially loaded columns, a constant level of compression was applied at the top of the topmost element and the total Lagrangian geometrical nonlinearity included the P-delta effect. Pullout of the reinforcing bars at the column-footing joint was taken into account by using a link element between the fixed support and the bottommost frame element, which was analyzed using the *exact bond pullout model* [10].

The analytical and experimental results for columns 1-4 are shown in Figure 12. In column 1, spalling of the cover concrete occurred when the applied displacement reached 15 mm, which was

very close to the value observed in the experiment. In the experiment, a gradual decrease in the lateral load could be observed after initiation of cover spalling. On the other hand, the analysis showed a sudden decrease in the load. This is because the spalling model abruptly ignored the strength of the cover concrete fibers once the nearby reinforcing bars experienced the spalling strain. In the analysis, buckling took place during the last loading cycle, as was the case in the experiment. It was found that the analysis could predict the post-peak softening behavior as well as the slight pinching in the cyclic loops, and the results of the analysis were closer to the experimental results in spite of the small difference in the peak load.

For column 2 also, the results of the analysis and experiment were found to be in good agreement. Matching the facts of the experiment, spalling and buckling mechanisms did not appear in the analysis because the compressive strain in the reinforcement fibers were not large enough. Consequently, softening in the load-displacement relationship was not noticed even in the high-displacement range, in both the experiment and the analysis. Moreover, in the analysis, pinching was not observed and the higher energy dissipation capacity was prominent. However, the cyclic loops in the load-displacement relationship were found to be slightly larger in the analysis than in the experiment. It is noteworthy to mention here that in load reversal, buckling and spalling may occur in spite of a small compressive strain if the reinforcement plastic strain during tension is large. However, in the cyclic loop of the reinforcement model used in this analysis, buckling was assumed to be independent of the tensile strain in the loading history. In other words, only isotropic hardening was taken into account. Kinematic hardening in the cyclic model of reinforcement will be included in the near future.

Similarly, the analytical load-displacement curve for column 3 was found to be close to that observed in the experiment. In both the experiment and the analysis, the cyclic load-displacement curves passed through the vicinity of the origin, causing severe pinching and a smaller load at zero displacement, which ensured a smaller energy dissipation capacity. Agreeing with the instability observed in the experiment, the analytical load-displacement curve also showed a sharp reduction in the load after the applied displacement reached around 30 mm. As the reinforcing bars were located only at the center and no axial load was applied in column 4, the contribution of the reinforcement to the overall response was small and the shape of the overall cyclic loop followed that of the concrete material model adopted in the analysis.

However, the analytical response was observed to be very close to the experimental response. Analysis could capture the cyclic path as well as the release of the load-carrying capacity due to high compression of the concrete when the applied displacement reached around 45 mm. This could also be observed in the experimental response curve. Although residual displacement during load reversal was significant, the cyclic loops asymptotically followed the horizontal axis (zero-load line), resulting in a very small load at zero displacement. Consequently, the cyclic response showed a pronounced pinching effect and a smaller energy dissipation capacity.

#### 4.4 Detail analytical investigation

Figure 13 shows the load-displacement curves for column 5 in both the experiment and the analysis, along with the stress-strain history of a reinforcing bar and the moment contributions of the reinforcement and the concrete fibers, which were obtained from the FEM analysis. As mentioned earlier, the experimental load-displacement curve passed very near the origin during unloading and reloading, which is unlike the response of normal RC columns. In order to understand the cause of this behavior, nonlinear finite element analysis using fiber model was carried out. Figure 13 shows that the overall responses in both analysis and experiment are very similar, although the residual displacement predicted by analysis is slightly smaller than that observed in the experiment. The stress-strain history of one of the reinforcement fibers is also shown in Figure 13, which illustrates that the reinforcement has already yielded.

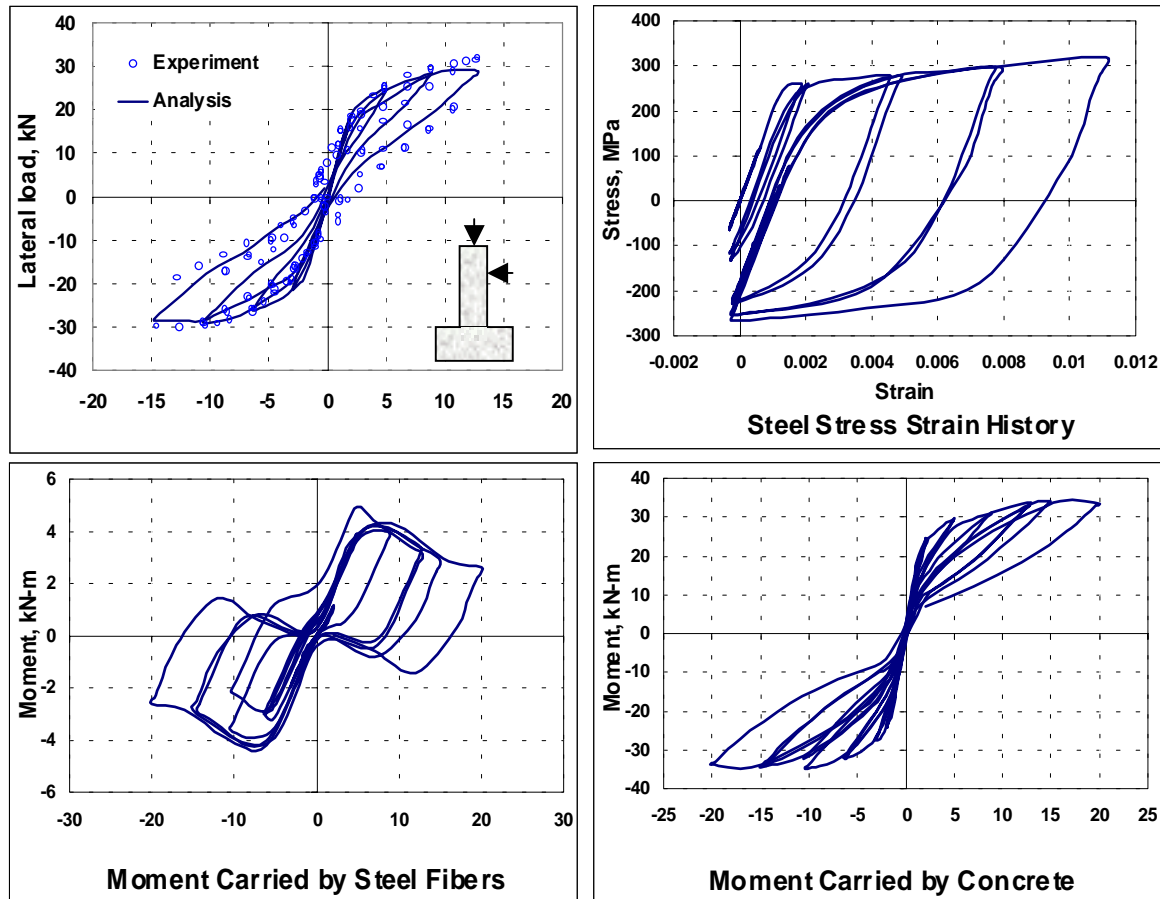


**Figure 13** Analytical results of column 5

Despite reinforcement yielding, however, the cyclic loops of the load-displacement curve (both in experiment and analysis) were very narrow and showed high pinching. The moment at the fixed support was then divided into two parts: that carried by the steel fibers and that carried by the concrete fibers. As can be seen in the figures, the moments carried by the reinforcement and the concrete at around zero displacement during reloading and unloading are very small. It is well known that the residual displacement and energy dissipation capacity in the load-displacement relationship of such structures come mainly from the reinforcement. In this case, however, unlike with standard structures, the contribution of the steel is around 1/10 that of the concrete. This is due mainly to the small reinforcement ratio and the small arm length, which is the result of the large cover. Apart from this, the steel itself exhibited a response with high pinching in the small-displacement range due to the presence of high axial compression. Hence, the overall response was very similar to the cyclic path of concrete fibers.

Cyclic analysis was further done for higher loadings, and one loop with applied displacement from 20 mm to -20 mm was investigated in greater detail. Figure 14 shows the average strain distribution and force carried by the fibers along the column cross-section at three instants (at two opposite peaks and at zero displacement). The discrete dot points shown in the force distribution curve represent the normal forces carried by the reinforcing bars at the corresponding locations. As expected, the strain distributions are linear, and even at zero displacement, there is compressive strain throughout the cross-section due to axial compression. Consequently at zero displacement, all the fibers are in compression and the force distribution (in both the concrete and the steel fibers) is nearly symmetrical, resulting in a small moment inducing a very small load at zero displacement.

In contrast, the force distributions at extreme displacements indicate that the forces carried by the reinforcement fibers in the two sides have different signs. A high compressive force is carried by

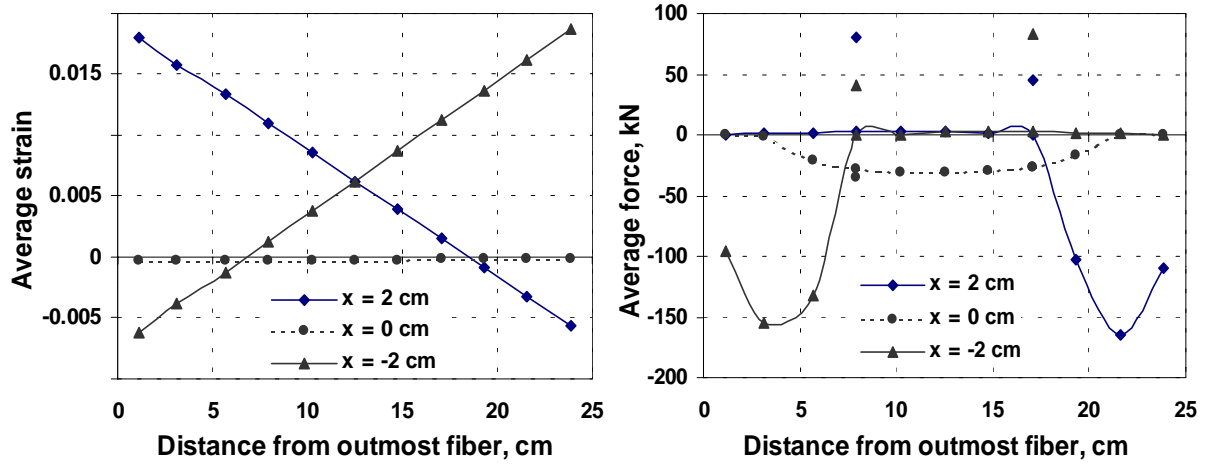


**Figure 14** Strain and force distributions in fibers across the cross-section

the concrete fibers in one side while the other side carries a very small tensile force. As a result, both the concrete and the reinforcement contribute to create a significant amount of moment, and the corresponding lateral loads are also high. A similar tendency can be expected in every loop.

A similar analytical investigation was carried out for one more case. The basic geometrical and mechanical properties of this column are the same as those of column 5, but the cover thickness is 23 mm and there is no axial load. Figure 15 shows the analytical load-displacement curve, along with the separate responses of the steel and the concrete fibers, as well as the strain and force distribution across the cross-section for three instants of one cyclic loop (applied displacement equal to 25 mm, 0 mm and -25 mm). As this figure illustrates, the cyclic response of the reinforcement shows wider loops without pinching due to the absence of axial compression, and

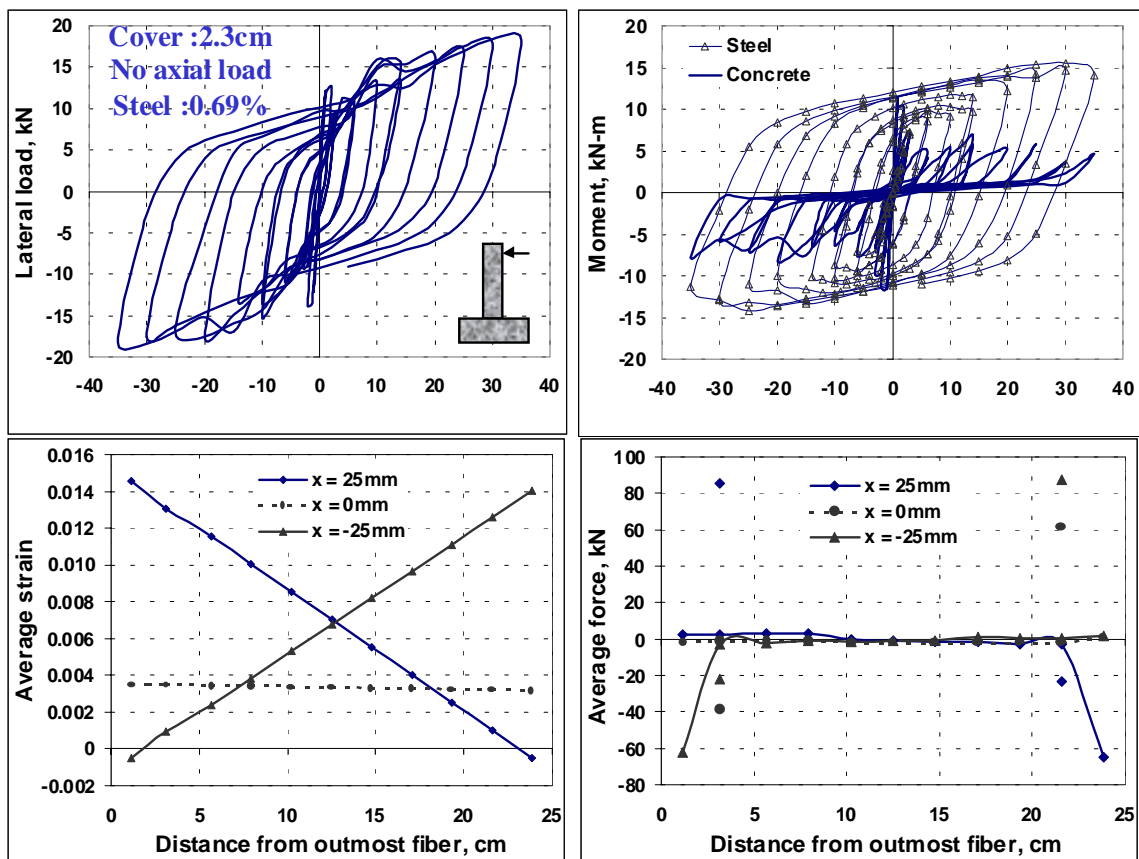


**Figure 15** Detail investigation of column without axial load and with small cover

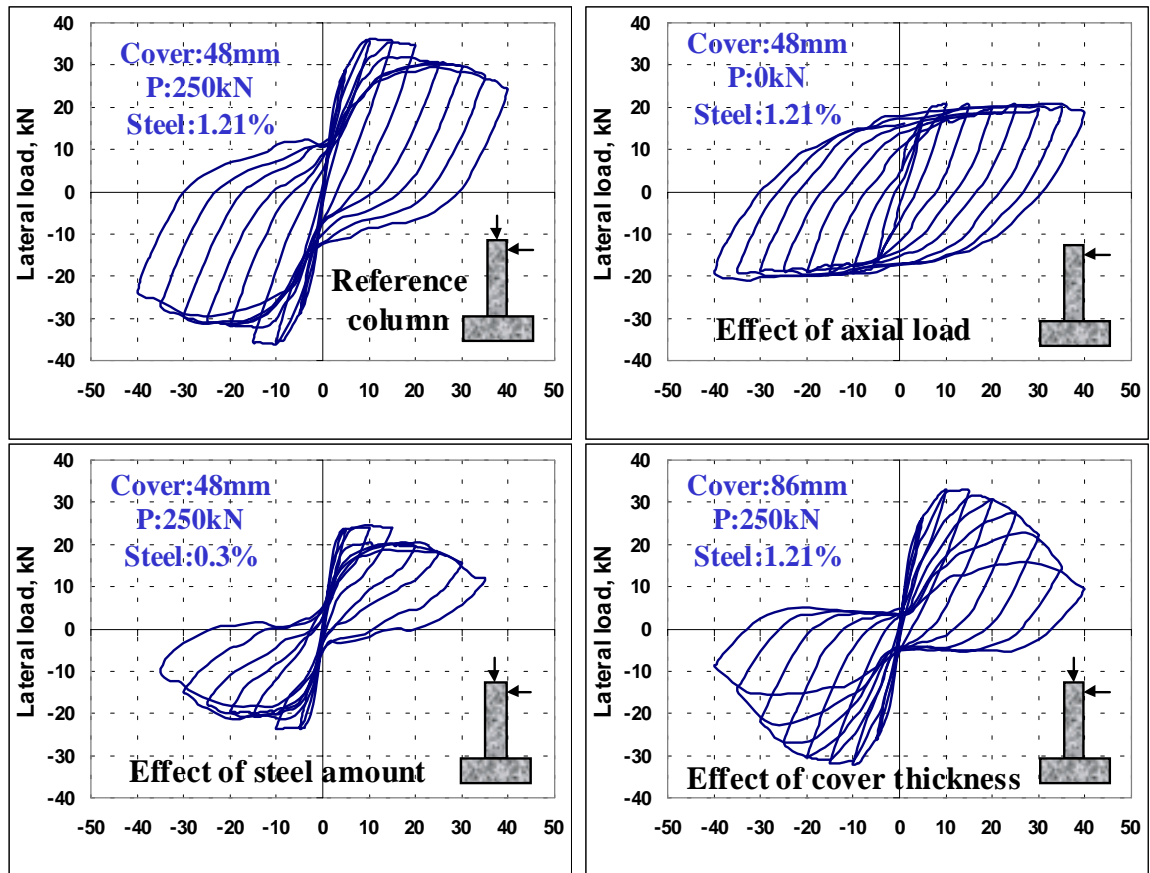


**Figure 16** Effect of axial load, reinforcement ratio and cover thickness in cyclic response

the relative contribution of the reinforcement to the section moment is significantly higher than that of the concrete. Consequently, the load-displacement curve for this column revealed a comparatively higher energy dissipation capacity. The strain and force distributions across the cross-section for extreme displacements are qualitatively the same as for column 5 except for the larger neutral axis depth.

However at zero displacement, there was a significant amount of tensile strain across the cross-section, and the forces carried by the concrete fibers were very small and symmetrical, ensuring a negligible contribution from concrete to the overall response at this instant. Obviously, to satisfy equilibrium conditions, the forces carried by the reinforcement fibers on the two sides are opposite in nature since no external load is applied. These opposite forces in the reinforcement contributed to the large section moment, producing a significant load at zero displacement.

#### 4.5 Parametric study

The above discussion shows that the post-peak response and energy dissipation capacity of RC columns depend on the cover thickness, the reinforcement ratio and the axial load. The qualitative interrelationship of these parameters and the post-peak cyclic response can now be analytically assessed. A rectangular column, geometrically similar to the tested columns, was considered. This column had the following material properties:  $f'_c = 30$  MPa;  $f_y = 350$  MPa;  $E_s = 200$  GPa. The reference column had a reinforcement ratio of 1.21%, a 48 mm thick cover, and 250 kN axial compression applied at the top of the column. For the other three columns, these parameters were modified in order to permit comparison with the reference column. Figure 16 illustrates the load-displacement relationships and the values of these parameters for the different columns. This figure reveals that the response of the reference column shows significant energy dissipation capacity with slight pinching. When the axial load is removed, the pinching disappears and the energy

dissipation capacity increases. Moreover, it can be observed that the energy dissipation capacity decreases and pinching becomes more severe as the reinforcement ratio decreases and also as the cover thickness increases.

A comparison of these four cases also provides a clear explanation of the post-peak response envelope. In the reference column, a sudden drop in the post-peak load due to cover spalling could be clearly observed. The post-peak response showed softening behavior due to the inelastic material nonlinearity (cover spalling and reinforcement buckling) and geometrical nonlinearity (P-delta effect). If the axial compression is removed, the P-delta effect disappears, and spalling and buckling do not occur. Consequently, the post-peak curve was stable. Reducing the amount of reinforcement produced higher post-peak softening because compression-softening of the concrete becomes more dominant as the contribution of the reinforcement becomes smaller. Last but not least, increasing the cover thickness accelerated the post-peak softening. Note that if the cover thickness is large, a comparatively higher curvature is required to induce the same strain in the reinforcing bars, which slightly delays both cover spalling and reinforcement buckling. However, once these phenomena occur, load degradation in the post-peak range is faster. In other words, the response is more brittle.

## **5. Conclusion**

Five reinforced concrete rectangular columns with different reinforcement ratios, cover thicknesses and axial loads were subjected to cyclic lateral displacements. Analyses were also carried out and it was found that coupled geometrical and material nonlinear finite element analysis reliably predicted the peak load, post-peak response, and cyclic loops with sufficient accuracy. The compression model of reinforcement, including the buckling mechanism that originally relates the average stress and average strain within the buckling length, was enhanced so that the overall computation would be independent of the element size in a finite element mesh. Based on fracture energy considerations, the post-yielding stiffness of the original buckling model was adjusted to obtain the average compression behavior of the reinforcement in the finite element domain. The proposed mesh size independent buckling model was proven valid with the help of finite element analyses of a fictitious RC column having different element sizes. Enhanced frame analysis using the cover spalling and reinforcement buckling models reliably captured the post-peak softening due to material and geometrical nonlinearity. The analytical results show that the post-peak response envelope and the cyclic loops are governed by the applied axial load, the reinforcement ratio and the thickness of the cover concrete.

## **Acknowledgement**

The authors gratefully acknowledge TEPCO Research Foundation and Grant-in-aid for scientific research No. 11355021 for providing financial support for this research.

## **References**

- [1] Dhakal, R. P. and Maekawa, K.: Behavior of laterally loaded RC columns with thick cover under axial compression, *Proceedings of JSCE Annual Conference*, Hiroshima, pp. 568-569, 1999.
- [2] Dhakal, R. P. and Maekawa, K.: Post-peak cyclic behavior and ductility of reinforced concrete columns, *Seminar on Post-Peak Behavior of RC Structures Subjected to Seismic Loads*, JCI, Tokyo, Vol. 2, pp. 151-170, 1999.
- [3] Menegotto, M. and Pinto, P. E.: Method of analysis of cyclically loaded RC plane frames including changes in geometry and non-elastic behavior of elements under normal force and bending, *Preliminary Report*, IABSE, No. 13, pp. 15-22, 1973.
- [4] Tsuchiya, S., Ogasawara, M., Tsuno, K., Ichikawa, H. and Maekawa, K.: Multi-axial flexural behavior and nonlinear analysis of RC columns subjected to eccentric axial forces, *Journal of*

*Materials, Concrete Structures and Pavements*, JSCE, No. 634, Vol. 45, pp. 131-144, 1999 (In Japanese).

- [5] Maekawa, K. and Okamura, H.: The deformational behavior and constitutive equation of concrete using the elasto-plastic and fracture model, *Journal of Faculty of Engineering, The University of Tokyo (B)*, Vol. 37, No. 2,, pp.253-328, 1983.
- [6] An, X., Maekawa, K. and Okamura, H.: Numerical simulation of size effect in shear strength of RC beams, *Journal of Materials, Concrete Structures, Pavements*, JSCE, No. 564, Vol. 35, pp. 297-316, 1997.
- [7] Okamura, H. and Maekawa, K.: *Nonlinear Analysis and Constitutive Models of Reinforced Concrete*, Gihodo, Tokyo, 1991.
- [8] CEB: RC Elements under Cyclic Loading - State of the Art Report, Thomas Telford, 1996.
- [9] Dhakal, R. P. and Maekawa, K.: Determination of buckling length of reinforcing bars based on stability analysis, *Proceedings of JCI Annual Conference*, Miyazaki, 2000.
- [10] Mishima, T. and Maekawa, K.: Development of RC discrete crack model under reversed cyclic loads and verification of its applicable range, *Concrete Library of JSCE*, Vol. 20, pp. 115-142, 1992.